We are IntechOpen, the world's leading publisher of Open Access books Built by scientists, for scientists

6,900
Open access books available

186,000
International authors and editors

200M
Downloads

Our authors are among the

154
Countries delivered to

TOP 1%
most cited scientists

12.2%
Contributors from top 500 universities

WEB OF SCIENCE™

Selection of our books indexed in the Book Citation Index in Web of Science™ Core Collection (BKCI)

Interested in publishing with us?
Contact book.department@intechopen.com

Numbers displayed above are based on latest data collected.
For more information visit www.intechopen.com

Chapter 3

MOCVD Grown HgCdTe Heterostructures

Pawel Madejczyk, Waldemar Gawron,
Artur Keblowski and Adam Piotrowski

Additional information is available at the end of the chapter

http://dx.doi.org/10.5772/62952

Abstract

HgCdTe heterostructures are widely applied for IR (infrared) detector constructing. Donor- and acceptor-doping researches in (100) and (111) oriented HgCdTe layers grown by MOCVD have been studied. Fully doped HgCdTe heterostructures with acceptor concentration range between 10^{14} and 5×10^{17} cm^{-3} and donor concentration range between 10^{14} and 1×10^{18} cm^{-3} and without post-grown annealing have been reported. The electrical and chemical characterizations of HgCdTe structures grown at 360°C on GaAs substrates using DIPTe have been described. Infrared photodiodes with different composition x were constructing on the basis of obtained heterostructures enabling signal detection of any wavelength from 1 μm to above 20 μm covering SWIR, MWIR and LWIR spectral ranges. Presented experimental results show that MOCVD technology enables to grow HgCdTe structures dedicated for HOT devices.

Keywords: HgCdTe, MOCVD, Doping, Heterostructure, infrared detector

1. Introduction

Mercury cadmium telluride $Hg_{1-x}Cd_xTe$ or MCT is a pseudobinary alloy whose development was commenced by Lawson and coworkers [1]. HgCdTe ternary compound is an excellent material for infrared detectors construction. Its position is conditioned by following characteristics:

- tunable energy gap allowing to cover the 1–30 μm wavelength range,
- advantageous intrinsic recombination mechanisms that direct to higher operating temperature (HOT),

INTECH
open science | open minds

© 2016 The Author(s). Licensee InTech. This chapter is distributed under the terms of the Creative Commons Attribution License (http://creativecommons.org/licenses/by/3.0), which permits unrestricted use, distribution, and reproduction in any medium, provided the original work is properly cited. CC BY

- high optical coefficients enabling high quantum efficiency.

Above-mentioned properties are simply consequence of the energy band structure of this zinc-blende semiconductor. The special advantages of HgCdTe are ability to obtain wide range of carrier concentrations, low dielectric constant, and high mobility of current carriers. The very small change of lattice constant with composition enables to grow high-quality layered and graded gap structures [2]. Thus, HgCdTe can be used for detectors operating at various modes [photodiode, photoconductor, or metal-insulator-semiconductor (MIS) detector].

This chapter reviews work from literature and some unpublished work from the authors' own laboratory that has been carried out into determining suitable extrinsic dopant species and sources for use in MOCVD growth of MCT heterostructures. The authors especially would like to present MOCVD technology with wide range of composition and donor/acceptor doping and without post-grown annealing as an excellent tool for (HOT) HgCdTe infrared photodetectors construction.

2. MOCVD grown MCT

MOCVD growth of MCT was firstly demonstrated in 1981 by Irvine and Mullin [3]. The reason for the delayed start in the growth of the mercury alloys in comparison to III–V compounds growth has been linked to the high mercury vapour pressures which needed some unconventional modifications to the MOCVD systems. MOCVD growth of MCT is determined by high vapour pressures of mercury that are necessarily to keep equilibrium conditions over the growing layer. This results from the instability of HgTe bonds in comparison with CdTe bonds and requires much lower growth temperatures than are typical for more stable compounds [4].

2.1. Thermodynamic considerations

The mercury chalcogenides are characterized by weak bonds of mercury what causes a higher equilibrium vapour pressure. If the evaporating species are Hg and Te_2, then the solid–vapour equilibrium is given by the following expression:

$$K = p_{Hg}\sqrt{p_{Te_2}} \tag{2.1}$$

where p_{Hg} is the equilibrium vapour pressure of mercury, p_{Te_2} is the equilibrium vapour pressure of Te_2, and K is an equilibrium constant which is a function of temperature. Eq. (2.1) implies that the equilibrium pressures of the component elements are linked and that there is a range of pressures over which the solid remains in equilibrium as a single phase. From the pressure–temperature phase diagram for HgTe presented in **Figure 1**, we can conclude that at MOCVD growth temperatures, the pressure can vary by three orders of magnitude and remain in equilibrium with a single phase of HgTe. However, it is clear from Eq. (2.1) that Te_2 partial pressure will be varying across this phase field in the opposite sense to the Hg partial pressure.

http://dx.doi.org/10.5772/62952

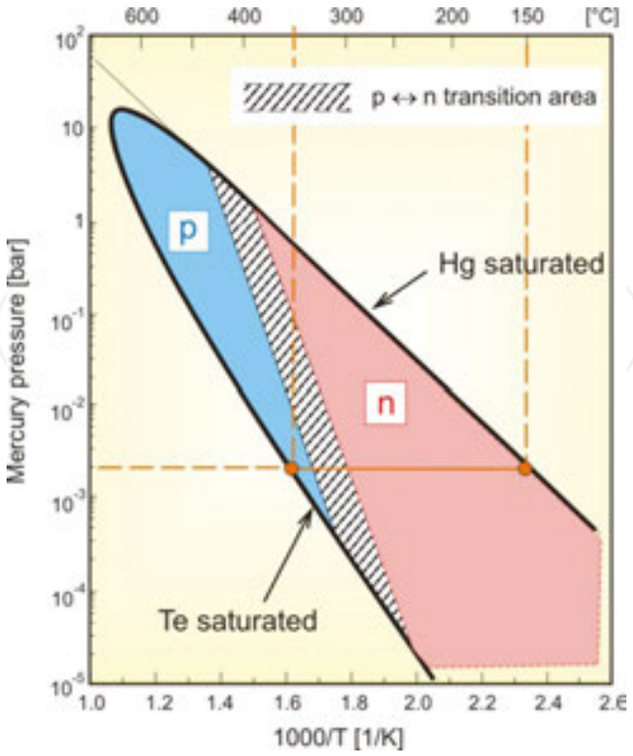

Figure 1. Mercury pressure–temperature phase diagram for HgTe. The p/n transition area indicates the transition from p-type to n-type for HgTe rich MCT annealed under equilibrium conditions [5].

The upper-phase boundary corresponds to the saturation of Hg over liquid mercury, and therefore, a horizontal line can be drawn from the equilibrium (pHg, T) to the intersection with the Hg saturated boundary in order to determine the equilibrium mercury source temperature. An example of a tie line is shown in **Figure 1** for the growth on Te rich-phase boundary at 350°C. If the HgTe layer is to be grown on Hg-rich-phase boundary, then the source and substrate temperature will be similar, which means an isothermal reaction cell. This is unacceptable for MCT MOCVD because Cd and Te organometallics will pyrolyse on the reactor cell wall before they reach the substrate.

The delivery of the vapour pressure of the Hg to the substrate for growth at 350°C must be greater than the minimum equilibrium pressure of 2×10^{-3} bar. In the author's system, the Hg source is an elemental mercury. The Hg partial pressure is about 30 mbar when the Hg zone temperature is maintained at 220°C during the IMP growth process.

2.2. MOCVD Growth approaches: IMP and DAG

There are two techniques for MOCVD growth of HgCdTe: the first based on direct growth of the ternary alloy—direct alloy growth (DAG) and the second based on interdiffused creation of the HgCdTe following initial deposition of alternating thin layers of CdTe and HgTe with total period thicknesses lower than 150 nm—interdiffused multilayer process (IMP). The latter technique takes advantage of the rapid interdiffusion rates ($D \sim 10^{-11}$–10^{-13} cm^2/s) of the cations in HgTe and CdTe at the typical growth temperatures in the range of 350–380°C. In IMP, the

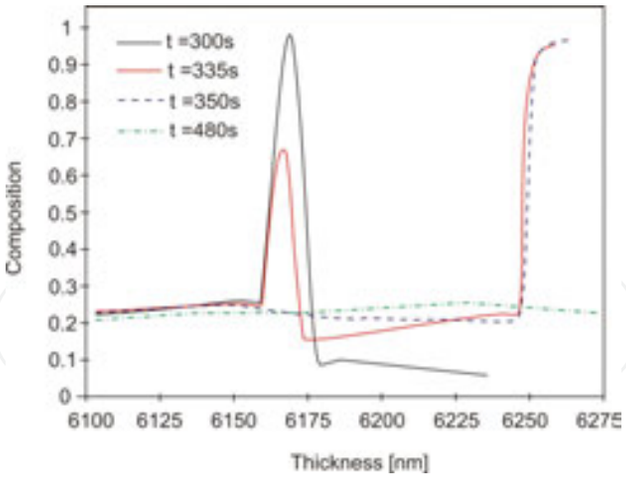

Figure 2. Composition profiles versus thickness modelled from laser reflectance data for a portion of an MOCVD-IMP growth run for x = 0.23 HgCdTe at different times (reproduced from reference [6]).

$Hg_{1-x}Cd_xTe$ final x composition is determined by the relative thickness of the HgTe and CdTe cycles which are easily monitored by controlling the times of their growth [4].

The sequence of four calculated compositional profiles for an IMP structure with 93.6 nm of HgTe and 27.6 nm of CdTe was presented on **Figure 2**. The cation interdiffusion process in IMP MOCVD growth technique of HgCdTe was demonstrated by monitoring the laser reflectance signal and modelling the IMP process. The HgCdTe was grown at 380°C. The first profile (the solid line) was taken at t = 300 s. It shows that formation of pure HgTe is inhibited by the fast diffusion of Cd atoms. The preceding CdTe layer is narrowing by interdiffusion but maintains composition x = 1 in the centre. The second period taken 35 s later is at the commence of the next CdTe growth phase, by which time the preceding CdTe layer has a maximum Cd composition of 0.6. The diffusion of Hg in CdTe is much slower than the diffusion of Cd in HgTe, and thus, the CdTe phase remains on the binary composition in the contrary to the HgTe phase. In the third time period taken 50 s after the experiment beginning, the x composition of CdTe layer has decreased below 0.3 and at after t = 180 s, entire structure is nearly completely homogeneous. The IMP growth technique is relatively ease in implementation, and its decisive advantage depends on the ability to control the Cd/Te ratio during the CdTe cycle of the growth. The dopants can be preferentially directed to the intended lattice site by controlling the Cd/Te ratio. Good uniformity in alloy composition and film thickness has been demonstrated by both techniques [7].

2.3. Growth mechanisms

A variety of different models have been used to describe the growth mechanisms of narrow bandgap II–VI semiconductors, and no clear mechanism has yet emerged from this research [4]. The haemolytic fission of alkyl radicals is a stepwise process where there is a different bond energy for the first and second radicals. In the case of DMCd, the bond energy is 193 kJ $mole^{-1}$ for the first methyl radical and 88 kJ $mole^{-1}$ for the second. The decomposition can simply be described by the following stepwise reactions where the first step is rate limiting:

$$(CH_3)_2Cd \rightarrow CH_3Cd^{\bullet} + CH_3 \tag{2.2}$$

$$CH_3Cd^{\bullet} \rightarrow CH_3^{\bullet} + Cd \tag{2.3}$$

More comprehensive study concerning HgCdTe growth mechanisms, you can find in references [4, 8].

2.4. Substrate type and orientation

The proper selection of substrate material and orientation has been a significant field for research in narrow gap II–VI semiconductors because it was recognized to be a limiting factor in the quality of the epilayers. Generally, we can divide substrates onto two categories: the first category is lattice matched II–VI substrates: CdZnTe and CdSeTe, and the second category is lattice mismatched substrates: GaAs, Si and sapphire (Al_2O_3). The CdZnTe ternary is expensive material, and it suffers severe segregation causing non-uniformity in alloy composition, and CdSeTe substrates have high impurity concentrations arising from the selenium source. Much of the MOCVD growth has concentrated on orientations close to the (100), normally with some misorientation to reduce the size of macro-defects, otherwise known as hillocks or pyramids. In a detailed analysis of the frequency and shapes of defects on different misorientations, it was concluded by Snyder et al. [9] that the optimum orientation was (100) 3°–4° towards the (111)B face. The most extensively used alternative substrate has been GaAs with a few microns of CdTe buffer layer reducing the 14% lattice mismatch between CdTe and GaAs. Most of the MOCVD growth onto silicon substrates has used a GaAs buffer layer to step the change in lattice parameter between silicon and CdTe. Substrate orientation as well as the HgCdTe orientation has been extensively reported to have fundamental influence on crystallographic defects, surface morphology, residual background concentration, and both donor- and acceptor-doping efficiency. **Figure 3** presents atomic arrangements of the (100) and (h,11)B surfaces on the (011) plane of HgCdTe structure. The HgCdTe crystallographic orientation influence on doping efficiency will be studied in next paragraphs.

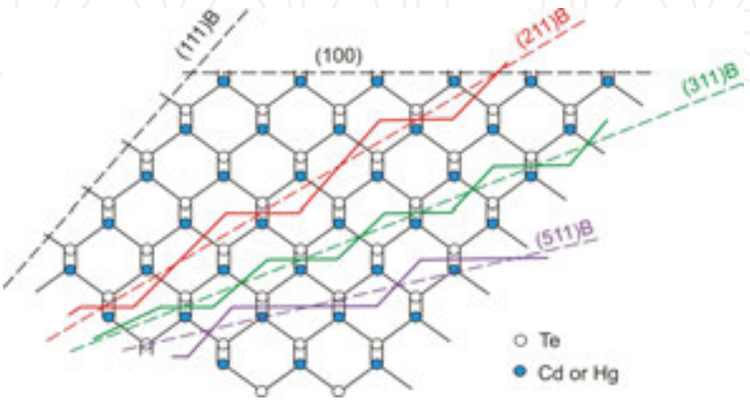

Figure 3. Atomic arrangements of the (100) and (h,11)B surfaces on the (011) plane of HgCdTe structure [10].

3. Growth of HgCdTe in Aix 200 system

HgCdTe epitaxial growth was carried out in the horizontal reactor of AIX-200 Aixtron MOCVD system (**Figure 4**). It consists of a horizontal rectangular aperture liner enclosed in an outer circular quartz tube. The system is designed to operate in the laminar flow regime with process pressures from 50 to 1000 mbar using a butterfly valve for pressure control. Reactor pressure of 500 mbar was used for all successful growth runs. Hydrogen is used as a carrier gas. Dimethylcadmium (DMCd) and diisopropyltelluride (DIPTe) are used as precursors. Ethyliodide (EtI) is used as a donor dopant source and TDMAAs (or AsH_3 in our previous researches) as an acceptor dopant source. DMCd and EtI are delivered through the one channel, while DIPTe and TDMAAs are delivered through the lower channel over elemental mercury bath.

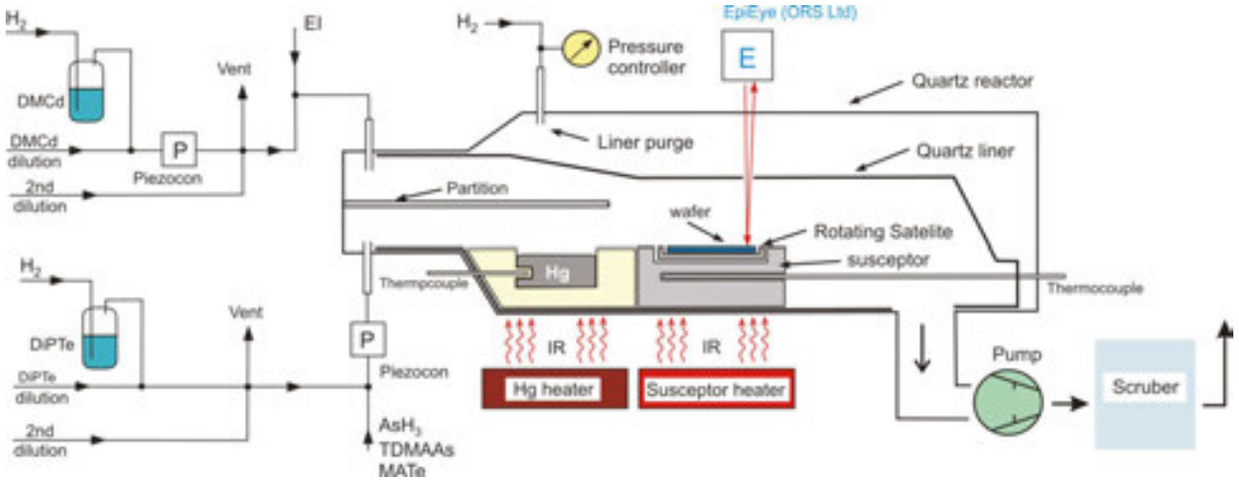

Figure 4. The scheme of the gas supply installation and the reactor in AIX 200 MOCVD system adapted to HgCdTe growth.

The Aixtron's gas foil rotation technique has been applied for better composition uniformity. There are two temperature zones in the reactor: the Mercury source zone and the growth zone with graphite susceptor controlled by external infrared heaters. High-temperature anneal was used before each growth run for reactor cleaning. Gas delivery system is additionally equipped with ultrasonic precursor concentration monitors—Piezocon and reflectometer—EpiEye. The usage of piezocons contributed to a better repeatability of the growth processes. Adaptation of EpiEye reflectometer allows for *in situ* monitoring. Typically, a 3–4-μm thick CdTe layer is used as a buffer layer reducing stress caused by crystal lattice mismatch between GaAs substrate and HgCdTe epitaxial layer structure. The buffer plays also a role of Ga diffusion barrier. The interdiffused multilayer process (IMP) technique was applied for the HgCdTe deposition [6]. HgCdTe was grown at 350°C with mercury source kept at 210°C. The II/VI mole ratio was kept in the range from 1.5 to 5 during CdTe cycles of the IMP process. An acceptor and donor doping has been examined over the wide range of compositions and doping levels of 5×10^{14}–5×10^{17} cm^{-3} have been obtained. Obtained HgCdTe heterostructures have been not annealed neither during the growth process (*in situ*) nor after the growth (*ex situ*) [11].

http://dx.doi.org/10.5772/62952

The set of metalorganic precursors gas supply suitable for Te and Cd delivery was presented in **Figure 5**. In our system, such a set supplies the reactor with DMCd and DIPTe. The H_2 carrier gas controlled by MFC (mass flow controller) is introduced into the bubbler and taking metalorganic precursor flows to the reactor. The bubbler is placed in the thermostatic bath. The liquid precursor temperature is one of the parameters determining precursor partial pressure in the reactor.

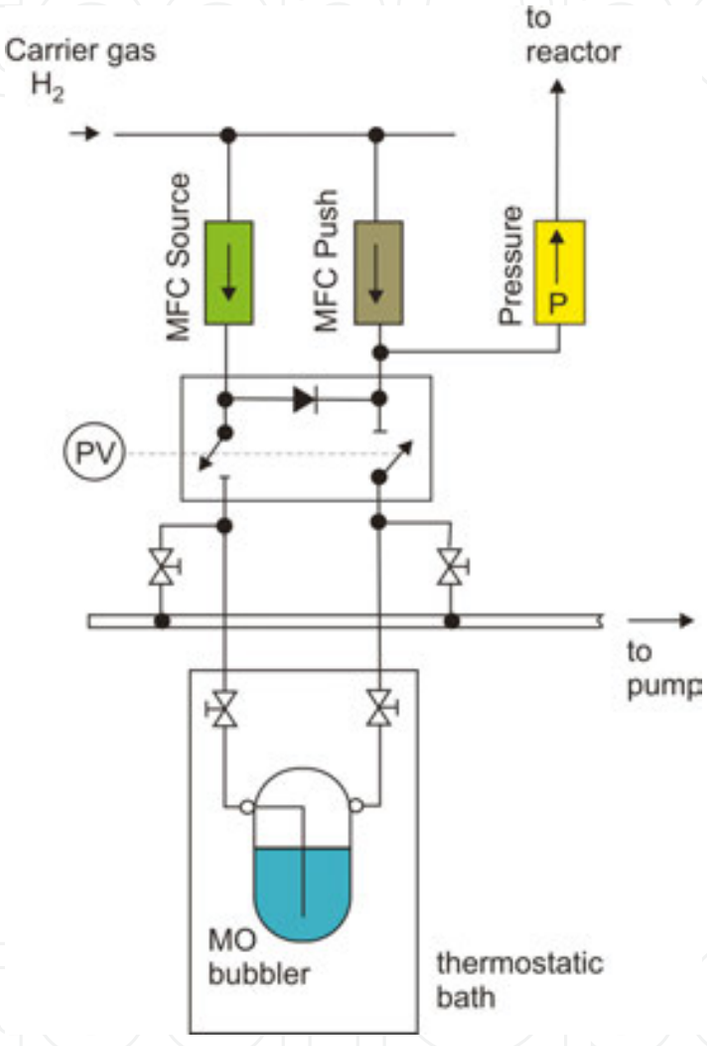

Figure 5. The set of metalorganic precursors gas supply suitable for Te and Cd delivery.

The partial pressures of cadmium and tellurium metalorganic compounds were calculated using following formulas:

$$P_p\left[mbar\right] = P_R\left[mbar\right]\frac{Q_{MO}\left[\frac{mol}{min}\right]}{Q_{Total}\left[\frac{mol}{min}\right]} \tag{3.1}$$

where Q_{Total} is the total gas flow through the reactor

$$Q_{MO}\left[\frac{mol}{min}\right] = \frac{Q_S}{22.4}.\frac{p(v)}{p_c - p(v)} \tag{3.2}$$

p_c is the pressure in the reactor, $p(v)$ is vapour pressure of the metalorganic in the bubbler, Q_S is the MFC source flow.

For metalorganic compounds, their vapour pressure is calculated using following formula:

$$Q_{MO}\left[\frac{mol}{min}\right] = \frac{Q_S}{22.4}.\frac{p(v)}{p_c - p(v)} \tag{3.3}$$

where T is bubbler temperature in Kelvins, and A and B are material constants shown in **Table 1**.

Material constant	**Metalorganic sources**			
	Cd	Te	EtI	Zn
A	1850	2309	1715	2109
B	7764	8288	7877	8280

Table 1. Material constant examples of the metalorganic sources.

In the author's system, the Hg source is an elemental mercury. The Hg partial pressure can be read from **Figure 1** and is about 30 mbar when the Hg zone temperature is maintained at 220°C during the IMP growth process.

The examples of surface morphology of obtained (111) and (100) oriented HgCdTe layers are presented in **Figures 6** and **7**, respectively. Both layers were not doped intentionally and are about 10 μm thick. The pictures were obtained using optical microscope with Nomarski contrast with ×1000 magnification. Both layers were grown on (100) GaAs substrate with 3° misoriented towards the (111)B face. The (111) CdTe buffer growth on (100) GaAs was obtained using Te flush during nucleation. The (100) CdTe buffer growth on (100) GaAs was obtained using Cd flush during nucleation. Both obtained layer are characterized by high uniformity in the composition and the thickness as well due to the Aixtron's gas foil rotation technique. It is clearly seen that the smoothness of (100) HgCdTe is much better in comparison with (111) HgCdTe what is attributable to microtwins on (111) orientation. The surface roughness coefficient Rq is equal 70 and 6 nm for (111) and (100) orientation, respectively. Rq coefficient was measured on Veeco optical profiler type Wyko NT 1100.

http://dx.doi.org/10.5772/62952

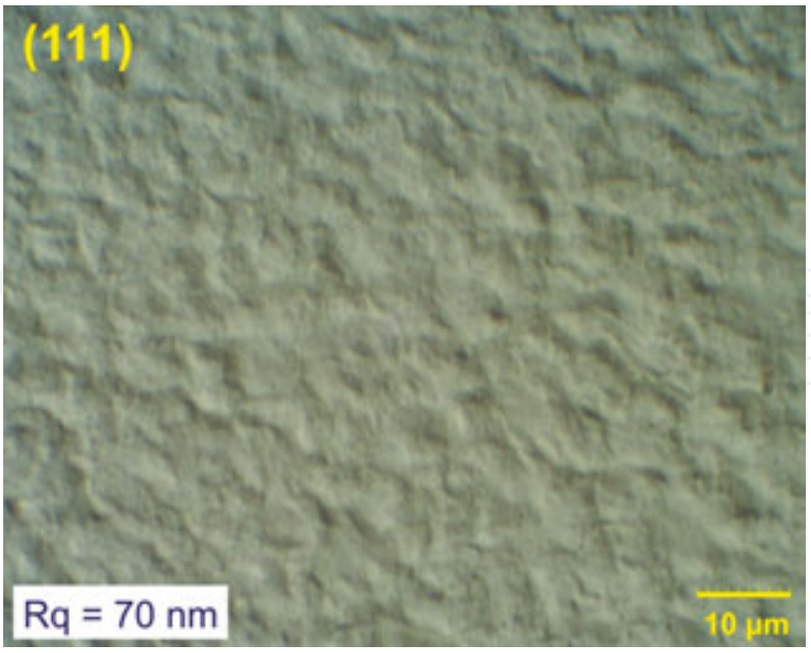

Figure 6. The example of surface morphology of obtained (111) oriented HgCdTe layer.

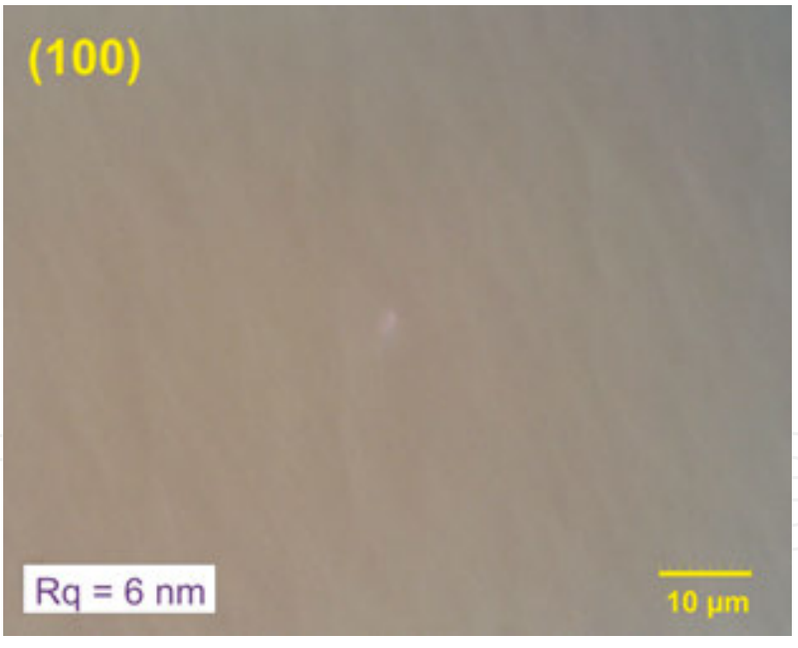

Figure 7. The example of surface morphology of obtained (100) oriented HgCdTe layer.

3.1. Undoped electrical properties

Indispensable in understanding the electrical properties of doped layers is the ability in interpretation of undoped layers results. The electrical properties of undoped MOCVD-grown MCT are dependent on the different parameters such as contamination from alkyls or

substrates [3, 12], crystallographic defects such as microtwins on (111) orientation, quench cooling conditions and native defects like mercury vacancies and others [13]. Although such defects do not affect interpretation of highly doped layers like contact layers, they may confuse interpretation of low-doped layers like absorbing layers in photodiodes structure. **Figure 8** presents residual background concentration of undoped HgCdTe layers versus consecutive number of growth processes carried out within 3 years in author's lab.

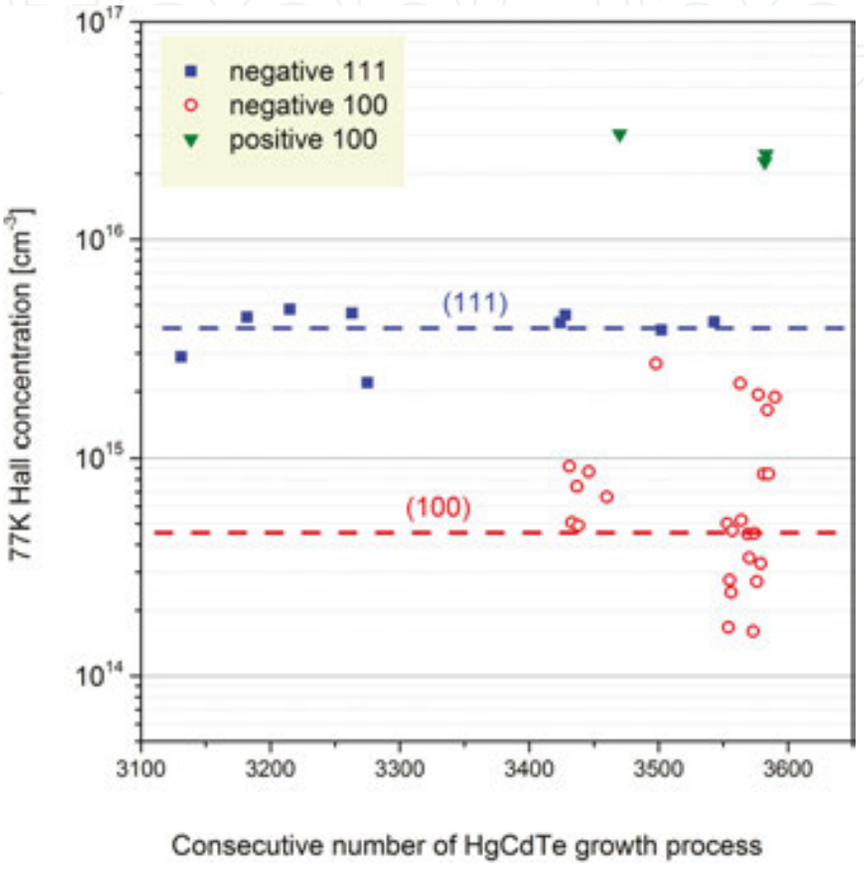

Figure 8. Residual background concentrations of undoped HgCdTe layers versus the numbers of growth processes.

The residual background concentration is a matter of huge concern of engineers form each semiconductor laboratory because it is the serious test of the equipment and applied materials purity as well as the result of the efforts of the staff. The mean residual concentration maintained in our laboratory is about 4×10^{15} cm^{-3} for (111) orientation and 4.5×10^{14} cm^{-3} for (100) orientation. An order of magnitude higher background concentration for (111) concentration is attributable to the microtwins presence. In the **Figure 8**, we can observe single points with positive (hole) concentrations above level of 10^{16} cm^{-3} for (100) orientations. These happened during experiments with lowering the mercury zone temperature in order to reduce the hillock density. Then, the mercury vacancies were created. The lowest background donor concentration obtained in our system is about 2×10^{14} cm^{-3} what is similar with the best results reported from other labs. The matter of residual donor concentration is particularly important during p-type doping at the low level.

http://dx.doi.org/10.5772/62952

4. Doping study

Improved performance IR photodiodes which require the growth of doped heterostructures have been theoretically modelled [14, 15]. Such structures require control of the dopant concentrations and sharp transitions between either dopant or different concentrations within a structure combined with bandgap changes induced by varying the alloy composition. To realize these doped junction structures, the dopants chosen need to have low diffusion coefficients at the growth temperature. Another considerable issue during doped heterostructures deposition is the control of any dopant memory effects. Some dopant sources may demonstrate 'run-to-run' memory effects in which the dopant is found to contaminate the run subsequent to the one in which the dopant was used. The dopant may induce memory effects within a single run which can limit the abruptness of the dopant transition. Then, the order of the layers within the structure can influence the sharpness of the electrical junction. Vast majority of papers concerning the influence of substrate orientation on impurity incorporation have pointed the complexity of the phenomena in play and have only given qualitative interpretations.

4.1. Donor-doping control

The selection for donor dopant in MCT is between the group III elements (Al, Ga, In) on metal sites and the group VII elements (Cl, Br I) on the Te sites. Despite some concerns over the diffusion coefficient of the group III species, these have been the most widely studied with most work concentrating on indium as the slowest diffuser of the group III elements [16, 17]. Although the reactive nature of the halogen elements, iodine doping has been studied at PRL [18] for the first time. The real aim of donor doping for the most device applications is to obtain control of the donor concentrations at $\approx 10^{15}$ cm^{-3} for absorbing layers and at $\approx 10^{17}$ cm^{-3} for n^+ contact layers.

4.1.1. Indium- and aluminium-doping studies

Trimethyl indium (TMIn) has been studied most widely as a doping source [13]. Despite its low vapour pressure, this source yields very high dopant incorporation. In incorporated preferentially into HgTe (20–50 times higher than in CdTe). This effect was use to attempt to lower the doping range by only injecting the TMIn during the CdTe cycles. However, the controllable doping range with a bubbler temperature of 2°C was still only from 2×10^{17} to 3×10^{18} cm^{-3}. Lower bubbler temperatures (-10°C) have been applied to obtain minimum concentration of 5×10^{16} cm^{-3} in MCT grown at 370°C using DAG. 'Effuser' mode bubbler operation with TMIn was investigated to dope at low level, but results were not promising. Although this did enable layers with $N_{D-A} = 2 \times 10^{16}$ cm^{-3} to be grown, the rate of increase in the donor concentration with bubbler temperature was very abrupt, making reproducible control very difficult. Similar rapid doping transitions were observed using a lower vapour pressure source [ethyldimethyl indium (EDMIn)] in bubbler mode meant that control of the donor concentration was only possible down to $\approx 10^{17}$ cm^{-3} [19]. This threshold effect was assigned to alkyl adsorption effects which were dependent on reactor design. Adsorption in the gas lines

and manifold can cause 'run-to-run' memory effects extended over several growth runs. The electrical properties of as-grown In-doped layers, which contain significant Hg vacancy concentrations, suggest that only 30% of the In is electrically active and that the In introduces additional Hg vacancies causing autocompensation in these layers [13].

4.1.2. Iodine-doping studies

The group VII elements, substituting on Te lattice sites, were expected to be slower diffusers. Preliminary researches of iodine doping in MOCVD were carried out with elemental iodine I_2. It has a vapour pressure of 0.3 Torr at 25°C. Electrically active donor incorporation was observed at low—10^{15} cm^{-3} doping levels with high mobilities. The proper control with abrupt doping profiles was not demonstrated, however, because I_2 reacts with DMCd. Improved doping efficiency has been expected when alkyl iodides were applied. In DAG deposition, iodine doping from isopropyl iodide has been reported to levels as low as 5×10^{15} cm^{-3}. However, isopropyl iodide introduced a memory effect. The initial choice for a MO iodide source was ethyliodide (EtI) due to its commercial availability. EtI is a highly effective precursor for doping without any memory effects [20]. Controlled iodine doping has been achieved in the range of 3×10^{14} –2×10^{18} cm^{-3} with 100% electrical activation following a standard Hg-rich stoichiometric anneal at 235°C. However, some works present similar donor-doping results without annealing. A double-dilution bubbler configuration is presented in **Figure 9**, and it has been used to obtain controlled low-level doping.

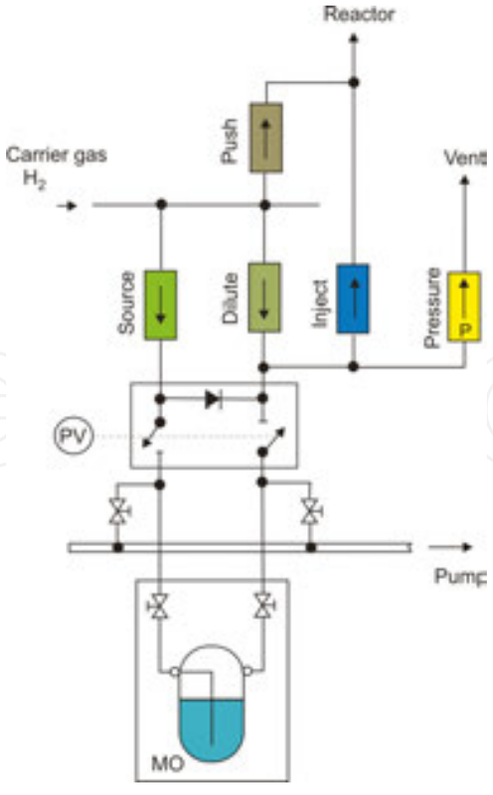

Figure 9. The double-dilution bubbler configuration for EtI doping.

The special doping structures contribute to reduce the number of growth experiments required to assess a doping source. Multilevel 'staircase' structures quickly yielded dopant source calibration curves and growth of a highly doped layer between two low-doped regions in a 'sandwich' structure yielded information on diffusion and reactor memory effects. **Figure 10** shows a 'staircase' (111) HgCdTe structure obtained using EtI which was assessed by SIMS and differential 77 K Hall profiling. Presented SIMS profile is shown from the growth perspective, while vast majority of such curves published in the literature are referenced from the layer surface. The errors in differential Hall concentrations become larger when the etch step size is around 2 μm. Consequently, it is very difficult to align the step positions with the grown layer interfaces. The correlation obtained between the chemical and electrical results implied the iodine incorporated on the correct Te lattice site; and that within the accuracy of the techniques, the activation efficiency is high. However, when we look at the **Figure 10**, the EtI-doping efficiency (the adjacency between chemical and electrical concentration) is decreasing with increasing dose level. This was corroborated by further layers, and **Figure 11** shows the resultant EtI calibration curve showing the linear control of both iodine and 77 K Hall concentration as a function of the injected EtI concentration in the reactor. For the comparison calibration curve for (100), HgCdTe layers is shown. We can see above one order of magnitude higher EtI-doping efficiency: incorporation and activation for (111)HgCdTe than for (100). The iodine should be located in the tellurium sublattice sites to act as a donor. The Te sides on the (111)B surface provide a more stable adsorption site with three bonds from the underlying group II atoms. On the contrary, the (100) surface provides a weaker adsorption site with two bonds (**Figure 3**).

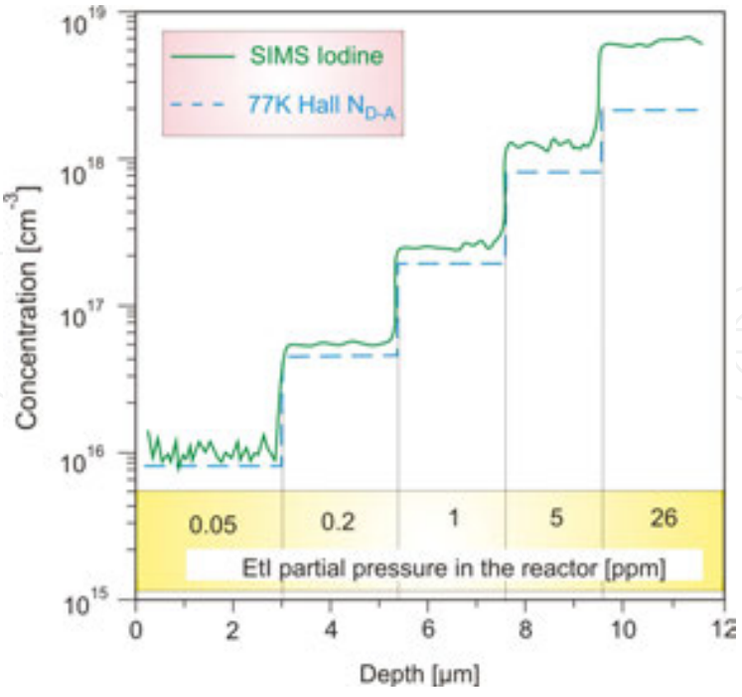

Figure 10. SIMS and differential excess donor concentration profiles of a 'staircase' (111) HgCdTe structure, doped using EtI [21].

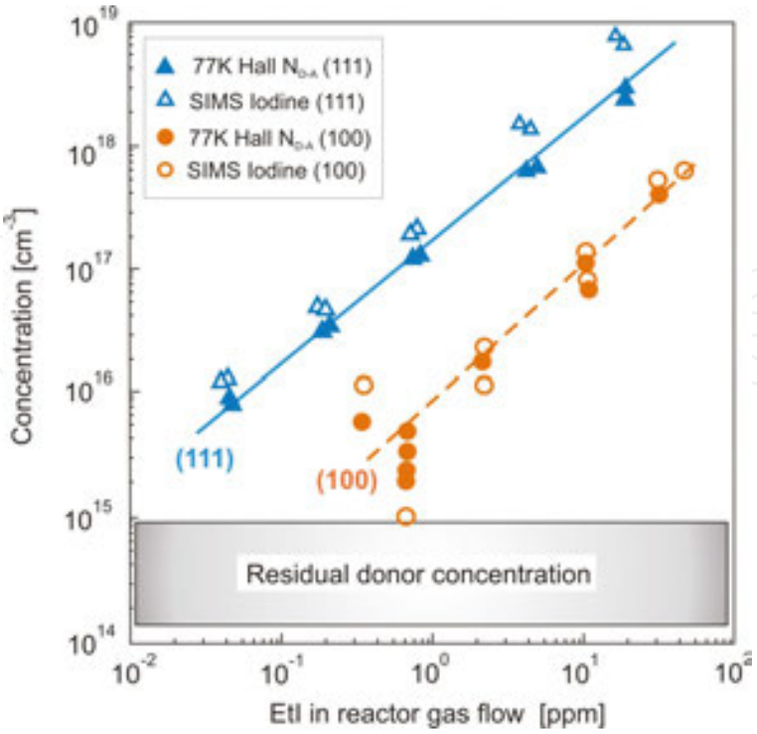

Figure 11. Calibration curve obtained with EtI for (111) and (100) oriented HgCdTe layers.

4.2. Acceptor doping

Acceptor doping should be provided by applying elements from the group IA (Li, Na, K), IB (Cu, Ag, Au) or group VB (P, As, Sb, Bi). The group I elements should be positioned on the metal lattice sites in order to provide theirs activity as the acceptors. The elements from group V need to be located on the tellurium sublattice sites. The group V elements are slower-diffusing species in HgCdTe and are versatile dopant capable of producing a variety of abrupt, doped junctions. If the group V elements were located on metal sites then they are likely to reveal donor behaviour. The most widely used element for acceptor doping is arsenic [22–28], although researches involving phosphorus and antimony have also been reported [13].

Figure 12 presents incorporation and activation of As from TDMAAs and AsH_3 versus precursor partial pressure for (111)HgCdTe. The chemical As concentration was determined by SIMS measurements. There is also comparison with 77K N_{A-D} (100)HgCdTe doped from TDMAAs. The As chemical concentration increases roughly proportionally with As precursor partial pressure up to 10 ppm. The levels of As incorporation from AsH_3 and TDMAAs into growing (111)HgCdTe samples are equal considering the measurement uncertainty. Arsenic precursors were introduced to the reactor during CdTe cycles of IMP growth process. The arsenic atoms appearance accelerates DMCd pyrolysis in the reactor that causes high shift in x composition. Chemical concentration of arsenic atoms measured by SIMS does not comply with acceptor electrical concentration determined by 77-K Hall measurements so we do not observe full arsenic activation. Also, for the same dose of arsenic in the reactor, the holes concentration in the (100)HgCdTe is about one order of magnitude higher than in

http://dx.doi.org/10.5772/62952

(111)HgCdTe. The arsenic incorporation considerably depends on crystallographic orientation. This dependence can be explained by considering that the two Cd and As atoms are readily active in the incorporation process. The created Cd–As species can break into on the surface if proper conditions are realized. In this respect, the (100) plane offers the best configuration because this surface has two double dangling bonds available for both Cd and Te (or substituting As) surface atoms (**Figure 3**). This mechanism can thus account for the highest doping observed with (100) substrates. Going away from (100) plane towards (111)A or (111)B leads to reduced As incorporation, and this corresponds to the fact that the relative fraction of (100) terraces decreases at the expense of (111) steps.

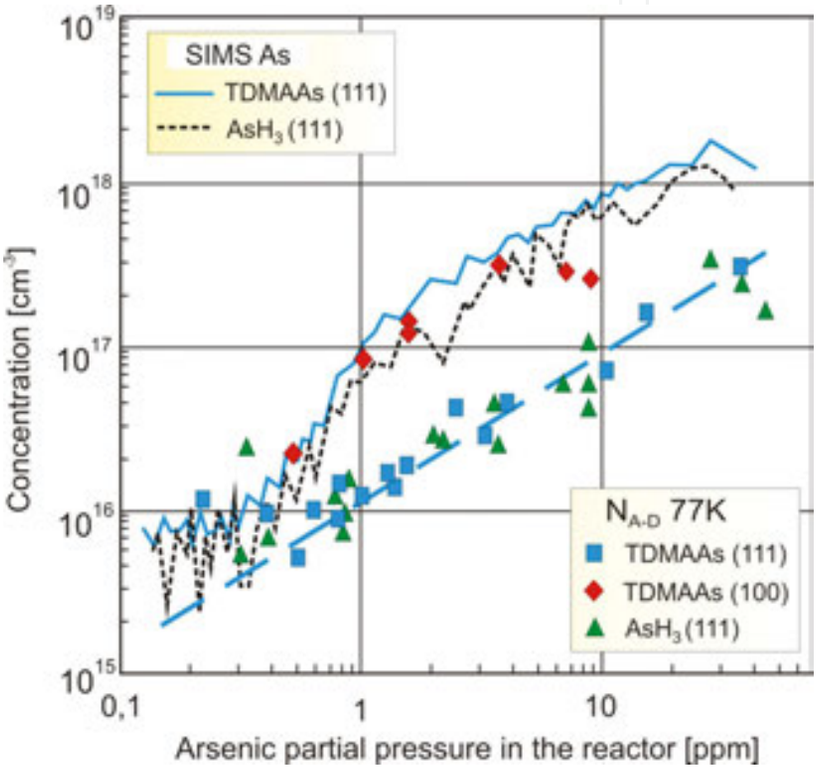

Figure 12. Incorporation and activation of As from TDMAAs and AsH_3 versus partial pressure of precursors.

5. Heterostructures and devices

After achieving device-quality MCT layers with doping control over the ranges required, the growth of doped junctions can be studied. When both donor and acceptor doping is required, for example in $P^+/\pi/N^+$ photodiodes, we prefer MCT with (111) crystallographic orientation because of limits with high-concentration doping control in (100)MCT. The capital letters P and N in device description means acceptor- and donor-doped layers with wider gap material. The upper index '+' denote high doping. If the particular device requires p-type doping only then is constructed on the basis of (100)HgCdTe. As an example, the MWIR photoresistors are presented in the Section 5.3. Cryogenic cooling of detectors has always been the disadvantage

of sensitive infrared (IR) systems. Conventional HgCdTe IR photodetectors should be cooled down below ambient temperature to reduce noise and leakage currents resulting from thermal generation processes. Presented in previous section progress in MOCVD technology let construct IR detectors operating without cryogenic cooling. Uncooled—operating in room temperature or thermoelectrically cooled devices—operating typically at 230 K is named as higher operating temperature (HOT) devices. The examples of IR HOT detectors operating in different IR spectral ranges are shown in the following sections.

5.1. LWIR photodiodes

The dark current in LWIR HgCdTe photodiodes is primary determined by Auger generation processes at elevated temperatures. The low-doped absorber layer becomes intrinsic, and the carrier concentration is higher than the doping level. The device structures with a combination of exclusion and extraction junctions in $N^+/\pi/P^+$ configurations have demonstrated suppression of Auger mechanisms by reducing the absorber carrier density below thermal equilibrium in a reverse bias condition. Classical $N^+/\pi/P^+$ structure has been expanded with graded interface layers denoted as 'G'. Graded doping and composition x layers represent the real structure which profile is shaped by interdiffusion processes during $Hg_{1-x}Cd_xTe$ growth at 350°C. Thus, $N^+/G/\pi/G/P^+/G/n^+$ HgCdTe photodiode structure has been obtained as it is shown in **Figure 13**. In order to improve electrical contact properties of metallization to P^+ layer, the structure was upgraded with p^+/n^+ tunnelling junction on the top.

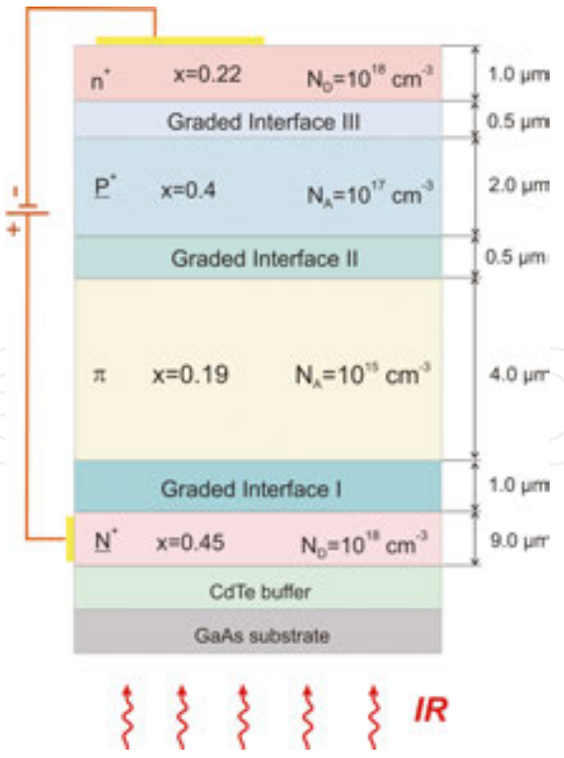

Figure 13. The LWIR $N^+/G/\pi/G/P^+/G/n^+$ HgCdTe photodiode diagram. x is the alloy composition, N_A—the acceptor concentration, and N_D—the donor concentration [29].

http://dx.doi.org/10.5772/62952

The cladding N^+-layer should be thicker than minority carrier diffusion length and doped at possible highest level providing reduction of series resistance. Analogously parameters of cladding P^+-layer are defined. The thickness of active π-type region (absorbing layer) should be shorter than minority carrier diffusion length. Generally, the thickness of absorber layer is a compromise between requirements of high absorption efficiency and low thermal generation. In our experiments, the thickness of absorber layer is varied from 3 to 6 μm. The acceptor doping of the absorber should be at possible low level just to overcompensate the donor background concentration of the material.

The SIMS profiles of $N^+/G/\pi/G/P^+/G/n^+$ heterostructure measured by CAMECA IMS 6F using positive and negative Cs ions are presented in **Figures 14** and **15**, respectively. The *x*-composition represented by the solid green lines has been calculated taking into account the measured SIMS points for Cd, Hg and Te elements. There is quite good convergence between projected and measured values in the absorber region. There are discrepancies between positive and negative ion measurements which result from incorrect SIMS ions calibration; about half of the order of magnitude differences between positive and negative ions for the arsenic-doping profile. The diffusion processes during the epitaxial growth cause gradient profile in the interface layers adjacent to the absorber region.

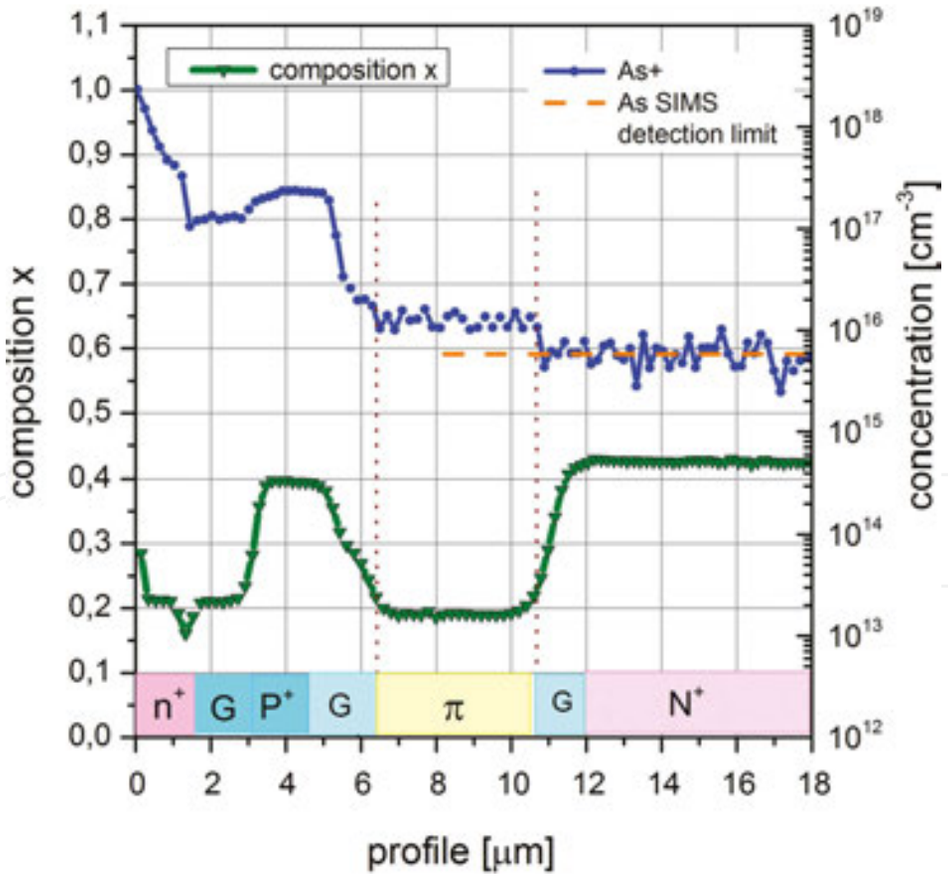

Figure 14. SIMS profile through $N^+/G/\pi/G/P^+/G/n^+$ (111)HgCdTe heterostructure measured by using positive caesium ions.

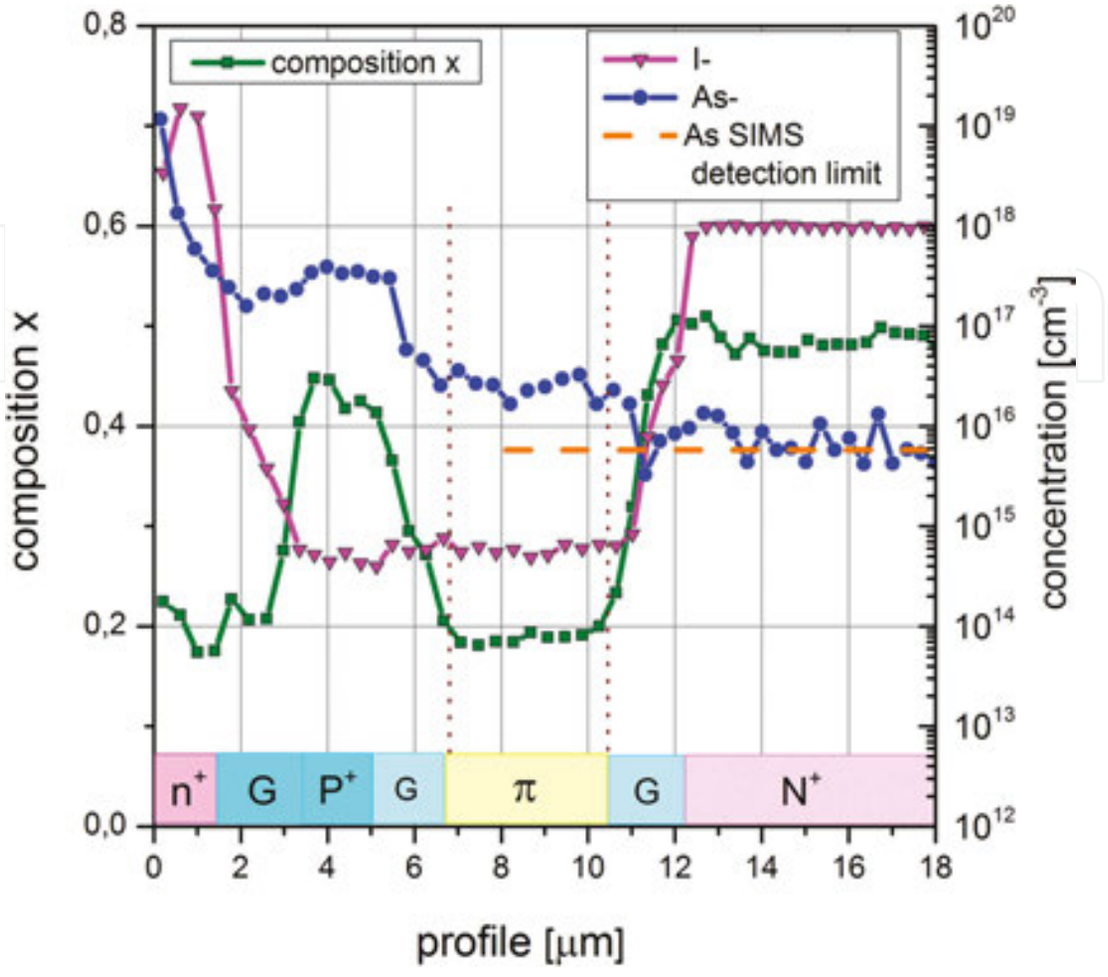

Figure 15. SIMS profile through $N^+/G/\pi/G/P^+/G/n^+$ (111)HgCdTe structure measured by using negative caesium ions.

The gradient slope of arsenic line between P^+ and absorber π-region seen in **Figures 14** and **15** indicates arsenic diffusion from P^+-region to absorber region what is dangerous especially in thin, 3-μm thick, absorber layers. The iodine profile (the solid pink line with triangles) seen in **Figure 15** indicates expected donor-doping levels: 1×10^{19} cm^{-3} for n^+-layer and 1×10^{18} cm^{-3} for N^+-layer with EI doses 90 and 19 ppms, respectively. Unwanted iodine presence in the absorber region is at the level of 1×10^{15} cm^{-3}, what is close to the SIMS detection limit for this element.

The $Hg_{0.81}Cd_{0.19}Te$ $N^+/G/\pi/G/P^+/G/n^+$ photodiode's current–voltage characteristic is presented in **Figure 16** for device with active region doped with 7 ppms of TDMAAs dose during the active layer deposition. Measurements were taken at 300 K (without any cooling) using the Keithley 2400 sourcemeter. The electrical area of devices is 8.1×10^{-9} m^2. The solid line denotes theoretically calculated results applying the *APSYS* simulation platform. The negative differential resistance between -150and -250 mV is attributable to the suppression of Auger processes due to the exclusion and extraction phenomena. The dark current is determined by both band-to-band (BTB) and trap-assisted (TAT) tunnelling mechanisms which evidences the quality of the material, for example the point defects like mercury vacancies. More comprehensive studies concerning fitting procedure have been reported in references [14, 15].

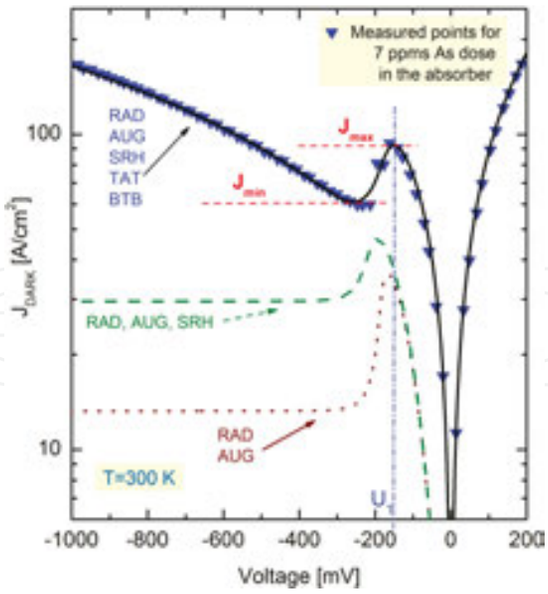

Figure 16. Modelled and measured characteristics of dark current density versus bias voltage for LWIR $N^+/G/\pi/G/P^+/G/n^+$ HgCdTe photodiode at room temperature [29].

The spectral characteristics have been measured at zero and reverse bias polarization using the Perkin Elmer FT-IR Spectrometer type Spectrum 2000. **Figure 17** presents the current responsivity versus wavelength for long wavelength $Hg_{0.81}Cd_{0.19}Te$ detector measured at 300 K. TDMAAs dose of 3.6 ppms was applied during the growth of the absorbing region. The values of the reverse biases are typically chosen considering current–voltage analysis and are typically beyond the threshold voltage U_T (designated in **Figure 16**). We can increase the current responsivity up to 50 times by the use of the reverse bias and thus causing Auger generation process suppression.

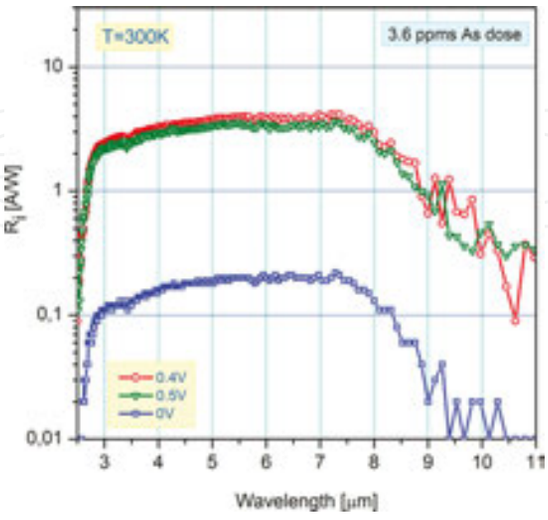

Figure 17. Current responsivity versus wavelength for LWIR HgCdTe photodiodes measured at room temperature [29].

5.2. MWIR photoresistors

The voltage responsivity versus wavelength for (100) and (111) HgCdTe MWIR photoresistors is presented in **Figure 18**. Photoresistors constructed from (100)HgCdTe have higher responsivity than these constructed from (111)HgCdTe. As it was discussed in the Section 4.2, there is higher acceptor-doping efficiency in (100)HgCdTe in comparison with (111)HgCdTe. However, presented values of the voltage responsivities are not fully comparable, because of the differences in $Hg_{1-x}Cd_xTe$ compositions in presented devices. The absorber composition in (100)HgCdTe was x = 0.337 whereas in (111)HgCdTe was x = 0.331. The cut-off wavelength λ_{CO} of measured photoresistors moves to longer waves with decreasing temperature because the energy gap is narrower.

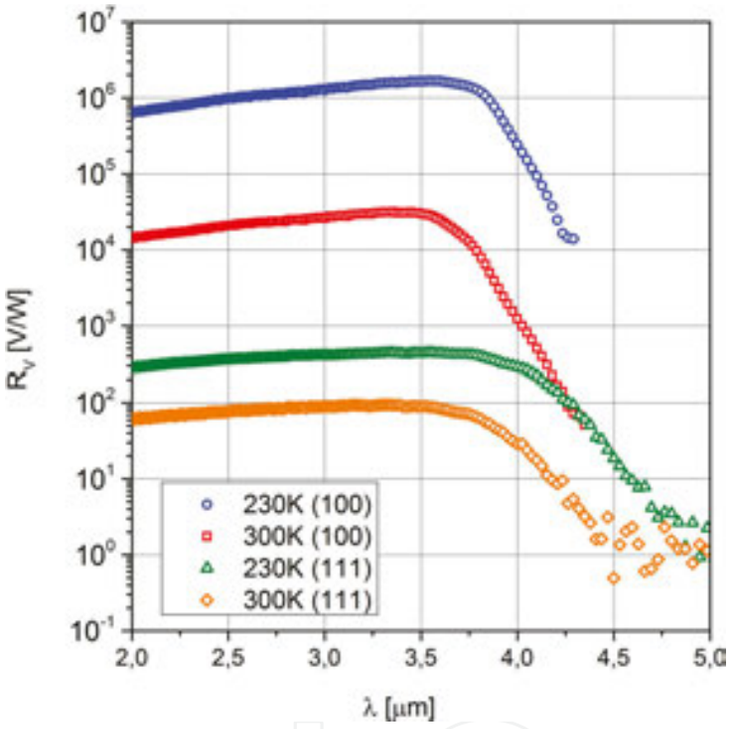

Figure 18. The voltage responsivity versus wavelength for (100) and (111) HgCdTe MWIR photoresistors.

6. Summary

In spite of other competitive technologies like InAs/GaSb superlattices, MCT material takes leading position in infrared detector industry at the time of writing this chapter. Donor- and acceptor-doping researches in (100) and (111) oriented HgCdTe layers grown by MOCVD have been studied. Fully doped HgCdTe heterostructures with acceptor concentration range between 10^{14} and 5×10^{17} cm^{-3} and donor concentration range between 10^{14} and 1×10^{18} cm^{-3} and without post-grown annealing have been reported. The electrical and chemical characterizations of HgCdTe structures grown at 360°C on GaAs substrates using DIPTe have been

described. Infrared photodiodes with different composition x were constructing on the basis of obtained heterostructures enabling signal detection of any wavelength from 1 μm to above 20 μm covering SWIR, MWIR and LWIR spectral ranges. Presented experimental results show that MOCVD technology enables to grow HgCdTe structures dedicated for HOT devices.

Acknowledgements

This study was supported by Polish National Science Centre as the Research Project No. UMO-2013/08/A/ST5/00773 and Polish National Centre for Research and Development as the Project No. TANGO1/2665576/NCBR/2015

Author details

Pawel Madejczyk[1*], Waldemar Gawron[1], Artur Keblowski[2] and Adam Piotrowski[2]

*Address all correspondence to: pmadejczyk@wat.edu.pl

1 Military University of Technology, Warsaw, Poland

2 VIGO System S.A., Ozarow Mazowiecki, Poland

References

[1] Lawson WD, Nielson S, Putley EH, Young AS. Preparation and properties of HgTe and mixed crystals of HgTe–CdTe. Journal of Physics and Chemistry of Solids. 1959;9:325–329. doi:10.1016/0022-3697(59)90110-6

[2] Rogalski A. Infrared Detectors 2nd ed. Boca Raton: CRC; 2011. 876 p.

[3] Irvine SJC, Mullin JB. The growth by MOVPE and characterization of $Cd_xHg_{1-x}Te$. Journal of Crystal Growth. 1981;55:107–115. doi:10.1016/0022-0248(81)90277-3

[4] Irvine SJC. Metal-organic vapour phase epitaxy. In: Capper P, editor. Narrow-gap II–VI Compounds for Optoelectronic and Electromagnetic Applications. 1st ed. London: Chapman & Hall; 1997. pp. 71–96.

[5] Jones CL, Quelch MJT, Capper P, Gosney JJ. Effects of annealing on the electrical properties of $Cd_xHg_{1-x}Te$. Journal of Applied Physics. 1982;53:9080–9092. doi: 10.1063/1.330419

[6] Svoronos SA, Woo WW, Irvine SJC, Sankur HO, Bajaj J. Model of the interdiffused multilayer process. Journal of Electronic Materials. 1996;25:1561–1571. doi:10.1007/BF02655400

[7] Mitra P, Case FC, Reine MB. Progress in MOVPE of HgCdTe for advanced infrared detectors. Journal of Electronic Materials. 1998;27:510–520. doi:10.1007/s11664-998-0007-5

[8] Bell W, Stevenson J, Cole-Hamilton DJ, Halis JE. Evidence for a surface-bound free radical mechanism during the decomposition of $^{i}Pr_2Te$ in the presence or absence of mercury and/or Me_2Cd under MOVPE conditions obtained from deuterium-labelled precursors. Polyhedron. 1994;13:1253–1265. doi:10.1016/S0277-5387(00)80259-4

[9] Snyder DW, Mahajan S, Ko EI, Sides PJ. Effect of substrate misorientation on surface morphology of homoepitaxial CdTe films grown by organometallic vapor phase epitaxy. Applied Physics Letters. 1991;58(8):848–850. doi:10.1063/1.104509

[10] Svob L, Cheye I, Lusson A, Ballutaud D, Rommeluere JF, Marfaing Y. Crystallographic orientation dependence of As incorporation in MOVPE-grown CdTe and corresponding acceptor electrical state activation. Journal of Crystal Growth. 1998;184/185:459–464. doi:10.1016/S0022-0248(98)80096-1

[11] Madejczyk P, Gawron W, Piotrowski A, Klos K, Rutkowski J, Rogalski A. Improvement in performance of high-operating temperature HgCdTe photodiodes. Infrared Physics and Technology. 2011;54:310–315. doi:10.1016/j.infrared.2010.12.036

[12] Madejczyk P, Gawron W, Piotrowski A, Klos K, Rutkowski J, Rogalski A. Influence of TDMAAs acceptor precursor on performance improvement of HgCdTe photodiodes. Acta Physica Polonica A. 2010;118(6):1199–1204.

[13] Maxey CD, GaleIG, Clegg JB, Whiffin. Doping studies in MOVPE-grown HgCdTe. Semiconductor Science and Technology. 1993;8:S183–S196. doi:10.1088/0268-1242/8/1S/042

[14] Martyniuk P, Gawron W, Madejczyk P, Rogalski A, Piotrowski J. Modelling of HgCdTe LWIR detector for high operations temperature conditions. Metrology and Measurement Systems. 2013;XX(2):159–170.

[15] Martyniuk P, Gawron W, Pawluczyk J, Keblowski A, Madejczyk P, Rogalski A. Dark current suppression in HOT LWIR HgCdTe heterostructures operating in non-equilibrium mode. Journal of Infrared and Millimeter Waves. 2015;34(4):385–390.

[16] Gough JS, Houlton MR, Irvine SJC, Shaw N, Young ML, Astles MG. The growth and properties of In-doped metalorganic vapor phase epitaxy interdiffused multilayer process (HgCd)Te. Journal of Vacuum Science and Technology. 1991;B9(3):1687–1690. doi:10.1116/1.585400

[17] Irvine SJC, Bajaj J, Bubulac LO, Lin WP, Gedridge RW, Higa KT. A new n-type doping precursor for MOCVD-IMP growth of detector quality MCT. Journal of Electronic Materials. 1993;22(8):859–864. doi:10.1007/BF02817498

[18] Easton BC, Maxey CD, Whiffin PAC, Roberts JA, Gale IG, Grainger F, Capper P. Impurities and metal organic chemical-vapor deposition growth of mercury cadmium telluride. Journal of Vacuum Science and Technology. 1991;B9(3):1682–1686. doi: 10.1116/1.585399

[19] Edwall DD. Comparison of spatial compositional uniformity and dislocation density for organometallic vapor phase epitaxial HgCdTe grown by DAG and IMP. Journal of Electronic Materials. 1993;22(8):847–851. doi:10.1007/BF02817496

[20] Maxey CD, Jones CL, Metcalfe NE, Catchpole R, Houlton MR, White AM, Gordon NT, Elliott CT. Growth of fully doped HgCdTe heterostructures using a novel iodine doping source to achieve improved device performance at elevated temperatures. Journal of Electronic Materials. 1996;25(8):1276–1285. doi:10.1007/BF02655020

[21] Madejczyk P, Piotrowski A, Gawron W, Klos K, Pawluczyk J, Rutkowski J, Piotrowski J, Rogalski A. Growth and properties of MOCVD HgCdTe epilayers on GaAs substrates. Optoelectronic Review. 2005;13(3):59–71.

[22] Vydyanath HR. Mechanisms of incorporation of donor and acceptor dopants in (Hg,Cd)Te alloys. Journal of Vacuum Science and Technology. 1991;B9(3): 1716–1723. doi:10.1116/1.585405

[23] Tascar NR, Bhat IB, Parat KK, Ghandhi SK, Scilla GJ. Extrinsic p-doped HgCdTe grown by direct alloy growth organometallic epitaxy. Journal of Vacuum Science and Technology. 1991;B9(3):1705–1708. doi:10.1116/1.585403

[24] Bevan MJ, Chen MC, Shih HD. High-quality p-type HgCdTe prepared by metalorganic chemical vapor deposition. Applied Physic Letters. 1995;67(23):3450–3452. doi: 10.1063/1.115276

[25] Song JH, Kim JW, Park MJ, Kim JS, Jung KU, Suh SH. Iodine and arsenic doping of (100)HgCdTe/GaAs grown by metalorganic vapor phase epitaxy using isopropyl iodide and tris-dimethylaminoarsenic. Journal of Crystal Growth. 1998;184/185:1232–1236. doi:10.1016/S0022-0248(98)80258-3

[26] Edwall DD, Bubulac LO, Gertner. p-type doping of metalorganic chemical vapor deposition—grown HgCdTe by arsenic and antimony. Journal of Vacuum Science and Technology. 1992;B10(4):1423–1427. doi:10.1116/1.586265

[27] Elliott J, Kreismanis VG. Orientation dependence of arsenic incorporation in metalorganic chemical-vapor deposition-grown HgCdTe. Journal of Vacuum Science and Technology. 1992;B10(4):1428–1431. doi:10.1116/1.586266

[28] Mitra P, Schimert TR, Case FC, Barnes, Reine MB, Starr R, Weiler MH, Kestigian. Metalorganic chemical vapor deposition of HgCdTe p/n junctions using arsenic and

iodine doping. Journal of Electronic Materials. 1995;24(9):1077–1085. doi:10.1007/BF02653056

[29] Madejczyk P, Gawron W, Martyniuk P, Keblowski A, Piotrowski A, Pawluczyk J, Pusz W, Kowalewski A, Piotriwski J, Rogalski A. MOCVD grown HgCdTe device structure for ambient temperature LWIR detectors. Semiconductor Science and Technology. 2013;28:105017–105023. doi:10.1088/0268-1242/28/10/105017

IntechOpen

IntechOpen